Peer-reviewed version available at Methods Protoc. 2018, 1, 39; doi:10.3390/mps1040039

*Article*

# Review of Biomedical Applications of Contactless Imaging of Neonates using Infrared Thermography and Beyond

**Abbas K. ALZubaidi [1,‡*], Yahya Ethawi [2,‡], Georg M. Schmölzer [2], Sherif Sherif [2], Michael Narvey [2] and Molly Seshia [3]**

[1] Biomedical Engineering Division, University of Saskatchewan, Saskatchewan, Canada
[2] Section of Neonatology, Winnipeg Regional Health Authority, Manitoba, Canada [3]
* Correspondence: aba658@mail.usask.ca; Tel.: +1-431-777-9679
‡ These authors contributed equally to this work.

**Abstract:** The monitoring of sick newborns is a challenging task that health care providers in Neonatal Intensive Care Units (NICU) must contend with each day. Conventionally, newborns are monitored via probes that are affixed to their skin and attached to processing monitors (Fig.1). However, an alternative exists in contactless imaging to record such physiological signals (Physio-Markers), surface changes and internal structures which can be used independently of, or in conjunction with conventional monitors. Advantages of contactless monitoring methods include: i) quick data generation; ii) lack of contact with skin, which reduces skin breakdown and decreases risk of infection; and iii) minimizing the number of probes and monitors affixed to the skin, which allows greater body surface-area for other care. This paper is an attempt to build a foundation for and to provide a vision of the potential neonatal clinical applications of technologies that use non-contact modalities such as Visible Light Imaging (VLI), Near InfraRed Spectrum (NIRS), and Thermal Imaging (TI) using InfraRed Spectrum (IRS).

**Keywords:** NICU; Physio-features; Neonatal imaging; Infrared thermography; Optical coherence tomography; Tissue optics; Near-infrared imaging; Short-wave infrared imaging; Visible light imaging

## 1. Introduction

Contactless imaging can be used to obtain a variety of vital signs to assess the health of a subject. Examples of these vital signs include heart rate (HR), respiratory rate (RR), body temperature, blood pressure (BP), peripheral vascular resistance (PVR), and cardiac output (CO). For the purpose of this paper, these vital signs will be referred to as “Physio-Markers” (PM), and their individual characteristic patterns will be referred to as “Physio-Features” (PF).


**Figure 1.** Standard monitors for a neonate inside an NICU.

### *1.1. Background*

Over the last three decades, contactless imaging in neonatal medicine has gained much attention, beginning with Clark's and Sothers' [1] first attempts to image preterm infants using infrared thermography. Clark's experiment opened the door to a variety of applications for contactless imaging. The experiment itself was simple, consisting of a single infrared camera mounted vertically on an incubator's Plexiglas hood to image the infant inside (see Fig.2). In the time since these first tests, several further investigations into contactless imaging's potential have been conducted using visible light, infrared, and ultraviolet (UV) spectra [1,2].

The difference between contact and contactless imaging is relatively simple: contact imaging involves the direct application of an imaging sensor to the subject's body (e.g. ultrasonography (US), electrical impedance tomography (EIT) [3,4], and bioimpedance tomography (BIS) [5,6]), while contactless imaging can detect, monitor, and visualize the subject's anatomy or physiology without direct physical contact, particularly with the skin. As there is no physical contact with the skin, contactless imaging is considered safer and has fewer associated complications than contact imaging [7–9].

Developing new contactless technologies, and optimizing existing ones, will lead to the creation of safer methods of diagnosing and monitoring preterm infants. In addition to being safer and having fewer potential complications, contactless monitoring may be a more cost-effective solution [10,11]. This article is part one of a two-part series, and it examines the technological aspects of contactless imaging approaches. The clinical applications of these technologies will be explored in part two.

Peer-reviewed version available at Methods Protoc. 2018, 1, 39; doi:10.3390/mps1040039



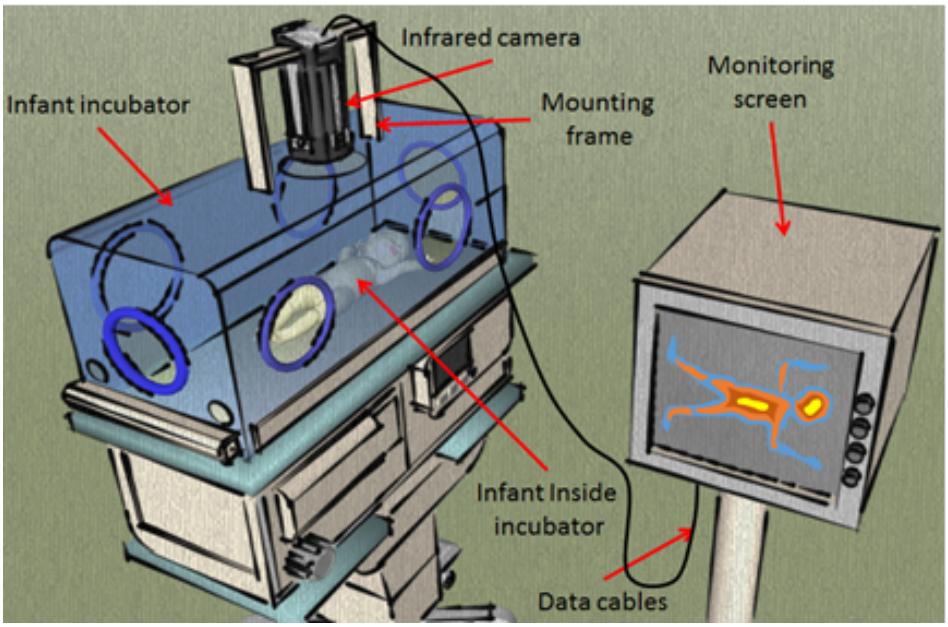


**Figure 2.** First contactless imaging set up used by Clark in 1980. This set up uses a traditional infrared camera with 5 frames per second (fps) and 5°C resolution

## 2. Contactless Neonatal Imaging Technologies

There are many contactless imaging technologies that may be potentially useful for solving different clinical problems. This section provides a non-exhaustive overview of some of the most promising contactless technologies that may be useful in an NICU setting.

### *2.1. Infrared Thermographic Imaging*

Infrared energy is part of the electromagnetic spectrum (see Fig. 3) and has similar properties to visible light: it propagates through space at the speed of light, and it can be refracted, reflected, emitted, or absorbed [2,12]. However, infrared wavelengths ($\lambda$) are longer than those of visible light—which are between 0.7 and 1000 $\mu$m—and infrared energy is associated with thermal effects [13–15]. The core temperature of the human body ranges between 36.5 and 37.5°C [11,16], while the surface temperature is approximately 33 °C [17]. Therefore, the range of human body temperatures that can potentially be recorded by a thermal (infrared) camera is between 33°C and 40 °C, which is equivalent to a wavelength in the range of several micrometers ($\mu$m) [18].

The mapping of human skin temperature, commonly known as thermal imaging, is currently used in clinical practice and medical applications [19,20]. These thermal images need to be processed if they are to provide meaningful information for clinical practice. Thermal imaging can detect several heat-energy-produced physiomarkers and physiofeatures that result from thermal-dynamic-induced events (cold or hot spots), for example, breast cancer [19,21] or local infections [22]. However, medical thermal imaging faces many challenges, such as standardized training to teach healthcare providers to interpret the images, and obtaining the necessary licensing from the appropriate regulating bodies.

Preprints (www.preprints.org) | NOT PEER-REVIEWED | Posted: 17 August 2018 doi:10.20944/preprints201808.0295.v1

Peer-reviewed version available at Methods Protoc. 2018, 1, 39; doi:10.3390/mps1040039



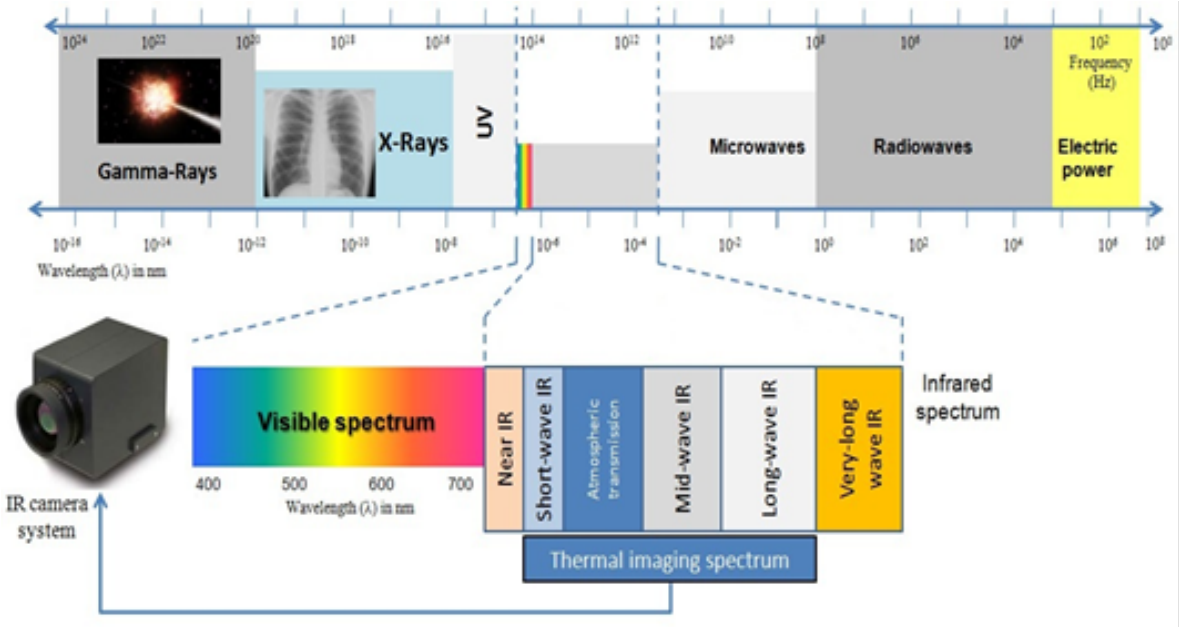


**Figure 3.** Electromagnetic (EM) spectrum showing infrared imaging band (reprinted with permission from one of the authors' previous work).

Basically, the infrared spectrum can be divided into five distinct regions according to the wavelength which can be summarized with their respective wavelengths as follows: i) Near-infrared (NIR) which has wavelength range between (0.7 $\mu$m – 1.4 $\mu$m), ii) short-wave infrared (SWIR) which has wavelength range between (1.4 $\mu$m – 3 $\mu$m) , iii) Mid-wave infrared (MWIR) which has a range of wavelength between (3 $\mu$m – 8 $\mu$m), iv) long-wave infrared (LWIR) which has a range of wavelength between (8 $\mu$m -15 $\mu$m) and v) far infrared (FIR), which has a range of wavelength between (15 $\mu$m – 1000 $\mu$m).

Table. 1 presents the most recent and relevant work in the field of infrared thermography imaging covering the whole IR spectrum, these works resemble the stand alone clinical and technical approach for integrating these technologies within the daily NICU workflow as part of smart neonatal incubator technologies. NIR is an imaging modality that can map the oxygenation status of body tissues—especially high-oxygen-utilizing tissues such as those found in the brain and the bowel—to provide information about their metabolic and functional activities [8,12,15]. NIR imaging is not simple due to living tissue's tendency to scatter light and also its anisotropic optical properties [28,36]. When the light propagates, it quickly diffuses throughout the tissue, as is shown in Fig.4. Therefore, it is not possible to image the internal absorbing structure by using a simple tomographic algorithm like those used in x-ray imaging [36]. Furthermore, the anisotropic structure will attenuate the light in a manner like absorption. Thus, it is difficult to differentiate the effect of absorption from the effect of scattering [37,38].

Peer-reviewed version available at Methods Protoc. 2018, 1, 39; doi:10.3390/mps1040039



**Table 1.** Overview of research using imaging modalities

| Approach /Technologies/Methods | Related work / research papers | Potential clinical applications |
|---|---|---|
| Infrared Thermography in Neonatal Thermoregulation | (Abbas & Leonhardt) [23] (Heimann) [8,23] (Knobel, Guenther, & Rice) [24] , (Saxena & Willital) [25] | Temperature & metabolism monitoring, peripheral blood perfusion, respiration detection. |
| Near Infrared (NIR) Imaging | (Blanik, Andropoulos, Arridge) [26–28] | Blood perfusion, Oxygen Saturation, cerebral blood flow, hemodynamic monitoring , brain injury, biomarkers imaging. |
| Short Wave Infrared Imaging (SWIR) | Langston [29], Dong [30] | Peripheral blood perfusion, blood vessels imaging. |
| Middle and Long Wave Infrared Imaging (MWIR, LWIR) | (Abbas & Leonhardt) [23], (Allen) [31], (Gade & Moeslund) [32] | Stress imaging, emotional classification, monitoring of temperature related physiology, and thermal imaging of the nostrils. |
| Photoplethysmography Imaging (PPG) | (Blanik) [26] | Hemodynamic monitoring, oxygen consumption monitoring. |
| Neonatal Imaging with Ambient/Visible Light Variation | (Nakamura) [33], | Monitoring of physiological signal such as heart rate, peripheral blood pressure and blood perfusion. |
| Embedding Contactless Imaging inside Incubator | (Abbas) [20] | Embedding of several physiological monitoring and imaging techniques inside the neonatal incubator such as (IR imaging, Magnetic impedance tomography (MIT) |
| Behavior and Emotional Monitoring of Neonate | (Gunnar) [34] (Vandenberg) [35] | Long-term monitoring and assessment of behavioral patterns of the neonates during daily care. |

Preprints (www.preprints.org) | NOT PEER-REVIEWED | Posted: 17 August 2018 doi:10.20944/preprints201808.0295.v1

Peer-reviewed version available at Methods Protoc. 2018, 1, 39; doi:10.3390/mps1040039



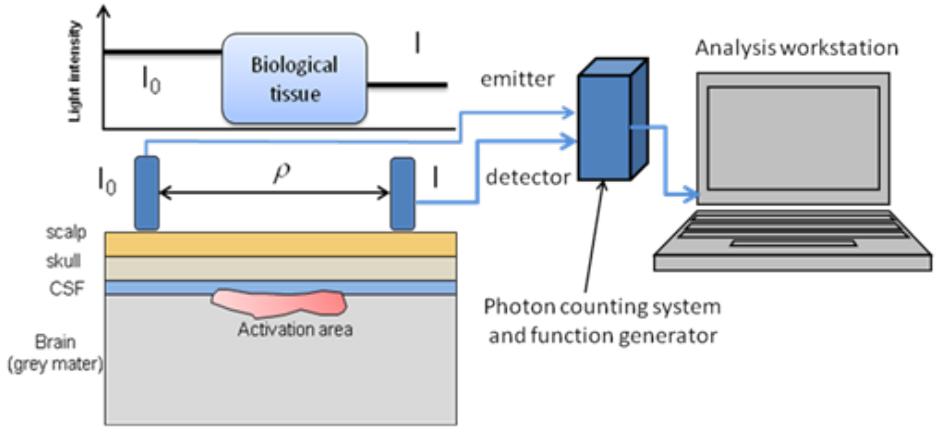


**Figure 4.** Basic mechanism illustration of the light absorption in NIR imaging of biological tissue

NIR imaging start with a pioneering modality known as optical topography, which uses a pair of single source-width=0.9 (SSD) attached to the scalp's surface to assess the function of a large surface area of the brain. However, this technique failed to provide adequate spatial resolution for imaging the internal structure of the brain [21,39–41]. Fig.5 shows another imaging modality, known as optical tomography, that generates two-dimensional (2D) or three-dimensional (3D) sectional images that are reconstructed to reflect the detail internal structure of the brain.

To date, topography and tomography have been applied to visualize the hemodynamics of the brain, with both being based on the measurement of flight times of photons traveling across the head. The distribution of photon flight times is unique and exclusive for each source-detector profile, and they provide sufficient information about the absorbance and scattering characteristics of light that is passing through the tissue.

The first 2D optical tomographic image of the brain was demonstrated by Benaron et al. [40] who developed an imaging system that measures photon flight times between various points on the head. Optical tomograms require multiple images, or slices of the brain, which are reconstructed using a straightforward back-projection method. This approach was used for detecting brain injuries in newborns, and could successfully demonstrate intracranial hemorrhages by detecting low oxygenated hemoglobin levels, which are a common characteristic of this condition.

A major drawback of this system is the simplicity of the image reconstruction algorithm, which ignores the inherent three-dimensional (3D) nature of photon migration in tissues and the highly-complex nature of an infant's head [42].

Another example of how NIRS can be applied in a medical context is to examine changes in hemoglobin-oxygen relation to assess the functional activity of high-oxygen-consuming tissues, such as the cerebral cortex []. In this application, an increase in afferent blood oxyhemoglobin (HbO) and a decrease in efferent blood deoxyhemoglobin ($HbCO_2$) are associated with changes in the local cerebral blood flow (CBF), which reflects the local perfusion and the oxygen consumption [44–46].

Peer-reviewed version available at Methods Protoc. 2018, 1, 39; doi:10.3390/mps1040039



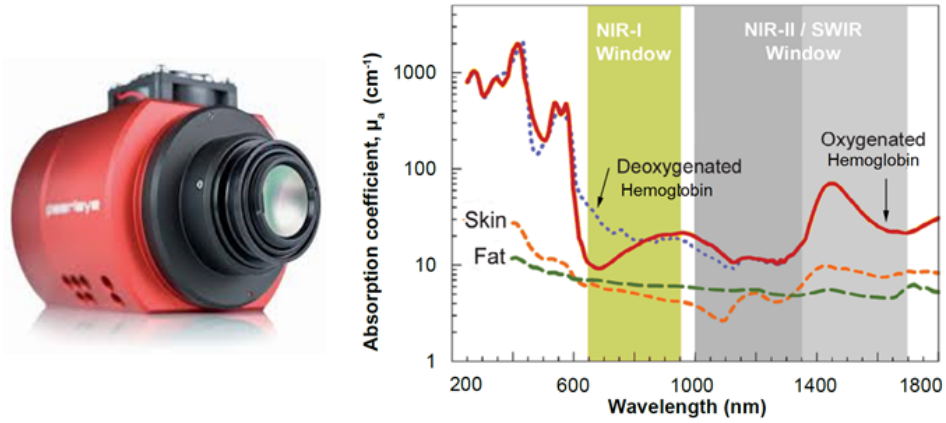


**Figure 6.** (Above) Example of an SWIR camera used in research and medical applications (courtesy of Stemmer Imaging Inc, Belgium); (Bellow) Absorption chart of light in tissue (Courtesy of Dr. Dominik J. Naczynski, Stanford University, adapted from Smith, A.M. et al. Nat Nanotechnology. (2009) 4, 710)

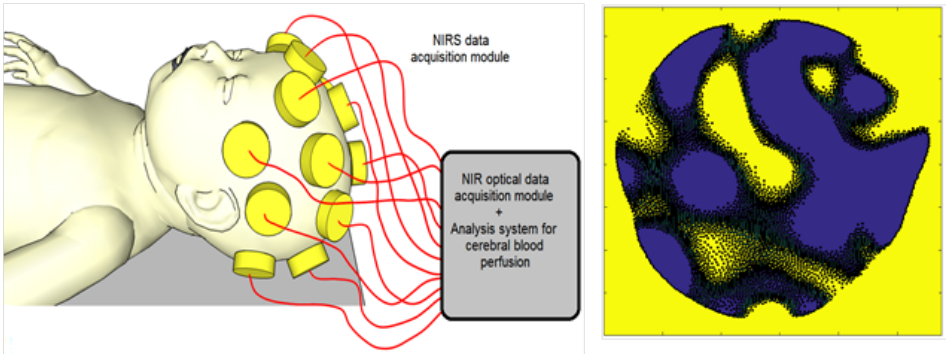


**Figure 5.** (Left) Diagram of neonatal NIR spectroscopy (NIRS) imaging. A series of photo-emitting diodes and photo-width=0.9 are integrated to acquire NIRS data from multiple areas of the neonate's head to reflect blood perfusion in the cerebral cortex. (Right) 2D reconstruction of NIRS images of a neonatal brain.

### *2.2. Short-Wave Infrared Imaging (SWIR)*

Despite the importance of SWIR imaging in medicine, its usage is very limited in neonatal monitoring. As shown in Fig.6, the SWIR wavelength band is located between 1 $\mu$m and 3 $\mu$m, which is also the band used for OCT imaging in tissues41, 42. The SWIR wavelength band passes through the scattering medium and can penetrate deeper than visible or NIR wavelengths. The imaging of the deep structures of biological tissues, which are optically opaque in nature, is the most challenging task for biological and clinical imaging. Optical imaging with visible light provides high resolution and sensitivity; however, the scattering and absorption of the light by the tissue limits the imaging depth to superficial structures. Imaging with SWIR shares many of the advantages of visible light imaging, but, unlike the last method, the scattering behavior of the tissue is reduced and significantly attenuated. Therefore, SWIR provides sufficient optical penetration depth to interrogate subsurface tissue features noninvasively [2,38,47].

Until recently, the potential applications of SWIR have been largely unexplored because suitable width=0.9 have either been unavailable or costly49. However, new detector technology offers the opportunity to demonstrate how SWIR imaging can be used to improve diagnostics. For example, SWIR scanning technology has been developed that can image the vascular system, and these images can provide valuable diagnostic information that can be used to complement the information obtained via Doppler ultrasound imaging, CT scans, or MRIs. SWIR light's ability to penetrate deeper tissue through the skin allows for better visualization of the human body, including the possibility of visualizing and detecting superficial vascular structures. Furthermore, SWIR's potential for detecting small-vessel structures has not been well-explored despite

Preprints (www.preprints.org) | NOT PEER-REVIEWED | Posted: 17 August 2018 doi:10.20944/preprints201808.0295.v1

Peer-reviewed version available at Methods Protoc. 2018, 1, 39; doi:10.3390/mps1040039



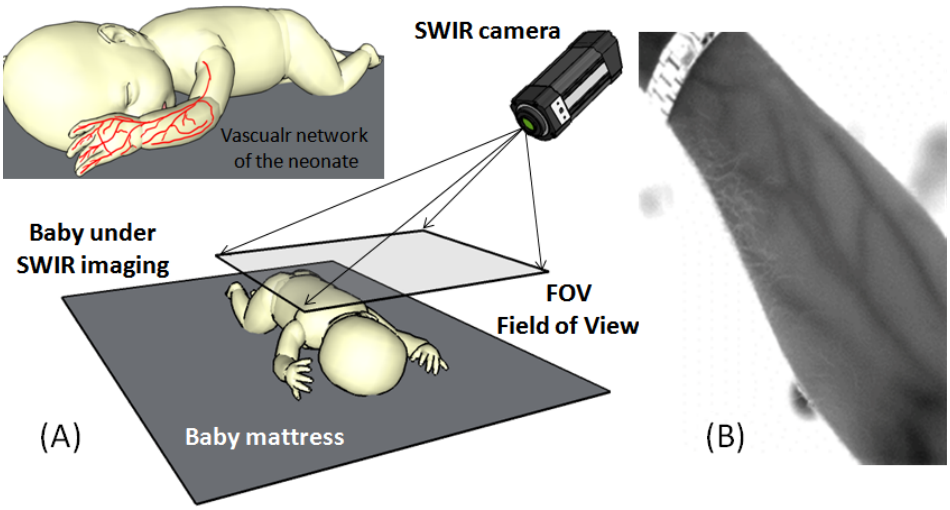


**Figure 7.** (A) Imaging setup of the SWIR with FOV set to cover the whole body of the neonate; (B) SWIR image of an adult hand showing the detailed vasculature of the forearm.

its potential usefulness for diagnosing complex vascular pathologies, such as hemangiomas and vascular malformations 48,49.

Fig.7 shows a typical SWIR imaging setup consisting of an SWIR camera positioned at a suitable distance from the neonate to acquire the field of view (FOV) of interest. The camera can be used with an external light source to illuminate the region of interest and to detect the light reflection rate through the SWIR width=0.9 [29,48]. Short waves spectrum has a limited ability to pass through the plexiglass of the incubator [1,20]. This limitation is due to the significantly degraded image (blurred, low resolution), low optical transmission rate (blurring of images associated with time) and temperature drift (inability of the camera to balance the difference between the temperature inside and outside incubator). SWIR spectral range camera is perfect for neonatal imaging because the spectral band deviated from $H_2O$ transmission absorption region (6 $mu$m – 7.5 $mu$m). Therefore, there is no need to put the SWIR camera inside the incubator or to use an optical window, such as a PE-foil or another optical filter to image the neonate while they are cared inside incubator.

### *2.3. Middle-Wave Infrared (MWIR) and Long-Wave Infrared Imaging (LWIR)*

There are several clinical implications within the range of MWIR and LWIR region. The thermal spectral band between 3 $mu$m - 14 $mu$m for MWIR and LWIR. Both have limited capabilities to pass through glass of the incubator due to degradation of the image (blurring). Therefore, the use of MWIR and LWIR are limited in neonatal clinical setting without the use of special optical windows (like: PE foils and IR transparent optical materials) [8]

The selection of MWIR and LWIR clinical application are based on other factors like the body's temperature distribution and dynamics, the circulatory system's regulatory mechanisms (vasoconstriction, vasodilatation, autoregulation, etc.), and the metabolic rates of different tissues [1]. The LWIR cameras are preferred for contactless imaging applications because it captures the absolute measurement (independent thermal point) or relative measurements (comparison of two points) of the thermal radiation of the newborn. The thermal energy of the newborn dominates other forms of the surrounding energy, because the characteristics of LWIR spectrum that is not present in other thermal spectral ranges (SWIR and MWIR).

Extreme care is required to ensure the radiometric measurement accuracy of the MWIR [14,66]. Finding a thermal reference during acquiring and converting MWIR thermal imaging is important as it provides thermal baseline points to limit detector to detector variation which improves measurement accuracy, rectangle, circle, triangle and sphere are examples of many thermal geometric references forms. These thermal references may include sources with temperature-controlled extended area or uniformly-coated metal plates that have contact temperature sensors [15,49].

Preprints (www.preprints.org) | NOT PEER-REVIEWED | Posted: 17 August 2018 doi:10.20944/preprints201808.0295.v1

Peer-reviewed version available at Methods Protoc. 2018, 1, 39; doi:10.3390/mps1040039



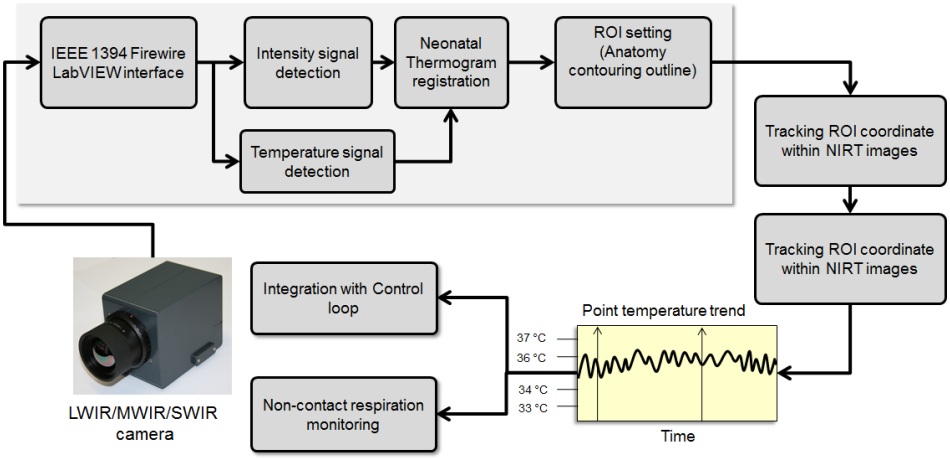


**Figure 8.** Block diagram of LWIR/MWIR and SWIR thermography processing in a computer-aided diagnosis system

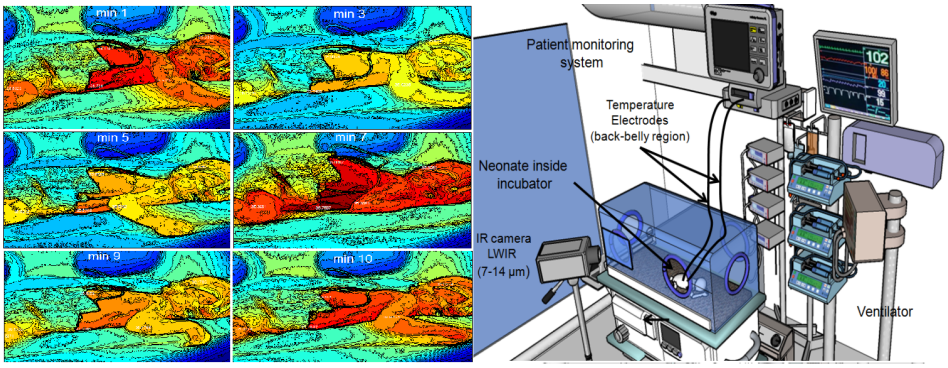


**Figure 9.** (Above) Typical experimental setup of neonatal infrared thermography (NIRT), including an LWIR camera and associated vital sign monitoring inside an incubator (closed-type); (Bellow) Sequence of the neonatal thermograms showing the evolution of temperature distribution over time (photos reprinted from previous work of the Author).

Fig.8 shows the block diagram of a modern thermography acquisition system. This system starts with recording the temperature or thermal imaging points then registers these points for the following steps. In these steps, several registered temperature points are used for the closed-loop control of the incubator, and temperature mapping and classification of thermal patterns of newborns.

Optical glasses with wavelengths ($\lambda$) ranging between 0.2 $\mu$m and 3.5 $\mu$m are transparent to light. This optical transmission then remains near zero level before the LWIR and very-long wavelength infrared (VLWIR) spectral regions [20].

There have been several attempts to use infrared thermal imaging to monitor the surface temperature of neonates. Fig.9 shows Abbas et al. [20,23] trial who used an LWIR camera for skin temperature registration and monitoring in different clinical scenarios. Another practical trial, performed by Knobel et al. [24] used infrared thermography to examine the relationship between the evolution of necrotizing enterocolitis (NEC) and body-core temperature in premature infants [50,51].

In practical terms, infrared thermography is highly significant because it provides a solid foundation for several pathological and clinical methods of monitoring an infant's body. For example, a surgical decision-making (SDM) module could be a significant aid in pediatric surgery. Monitoring in pediatric surgery requires dynamic revised updates based on assessments of the status and perfusion of the region of the body being operated on. The SDM module reconstructs the images in real-time to accurately reflect the extent of tissue necrosis of the relevant body region.

Peer-reviewed version available at Methods Protoc. 2018, 1, 39; doi:10.3390/mps1040039



### 2.4. Photoplethysmography Imaging

Several investigators developed photoplethysmography imaging (PPGI) prototypes for testing and validation inside clinical setting [52]. The essential component of the PPGI system is a remote-based camera for visualizing superficial vascular networks and detecting blood volume changes in different areas of a measured object [42,53]. PPGI uses the same fundamental principle to improve on the poor spatial resolution inherent to conventional skin contact PPG. Therefore, the PPGI technique can be used as a tool for monitoring skin perfusion in newborn infants [54].

Measurements of the skin's optical damping properties (0.4 $\mu$m to 0.7 $\mu$m of visible spectrum and 0.4 $\mu$m to1 $\mu$m of near infrared) are dependent on blood and tissue composition within the measurement pathway between the light source and the detector [26,28,55]. This structure is modulated by changes in blood volume in the venous and/or arterial systems in various patient-activity states [56,57].

Conventional PPG sensors consist of one or more light sources, usually light-emitting diodes (LEDs), and either a phototransistor (PT) or photodiode light detector (PLD) [23]. Depending on how these components are positioned, measurements are conducted either in transmissive mode (e.g. in clips for earlobes or finger tips) or reflective mode (e.g. adhesive sensors on the skin surface). PPGI measurements use a high-resolution camera with a multi-wavelength tissue illumination array instead of the singular contact sensor that is used today in pulse oximetry technology [58–60].

This measurement approach allows for contactless assessment of the tissue perfusion with the same spatial resolution as in the camera's field of view (FOV) [23,27,61]. Thus, every pixel of the camera's sensor array can be considered a discrete element of the PPG sensor, as the functional-imaging frame of the FOV assesses vital parameters by performing computation for predefined regions of interest (ROI) or each pixel separately [62,63].

The PPGI is suitable for measuring the same physiological parameters as PPG, including dynamic parameters [26,64,65]. Some examples of dynamic parameters include: capillary refill time, muscle pump efficacy, venous outflow, pulse characteristics (rate, variability, rhythm) [10,11,66], and arterial oxygen saturation. The main divergence between PPGI and PPG is in the composition of the measured light intensities and the number of elements used for detection [53,67].

The principal applications of PPGI are either simultaneous measurements of comparable locations in the body or inaccessible areas that require contact PPG sensors. One example of an instance where PPGI is useful for measuring inaccessible areas is in the assessment of skin perfusion reactions to allergy tests [48,64,68]. An additional potentially useful application of PPGI is to use a specially-mounted PPG camera, with its related lighting panel, inside a neonatal incubator to monitor allergy responses in the skin following a blood transfusion and other clinical interventional procedures [22,67,69].

### 2.5. Neonatal Imaging with Ambient / Visible Light Variations

Information can be detected and processed using ambient light reflection, scattering, and diffusion in human skin. The interpretation of photoplethysmography data or visible intensity variations can provide an explicit representation of human tissues. The data contains multiple projections of intensity changes, hue, saturation, and energy dissipation, which can provide additional information about the tissue being imaged. Several attempts have been made to develop an image/video processing algorithm for extracting and interpreting physical information related to the pixel value variation during the visible light video acquisition [35,41].

VLI is a robust and cost-effective method for analyzing the external cutaneous hemodynamic changes in the body. An example of these dynamics is observable in exposed skin vasculature where there is an insensible displacement recognized by rigid-motion detection within visible video recording as shown in Fig. 10 (right) which can be sued to detect pain, emotion, seizures and others. However, this method is hampered by the fluctuation of the ambient light and the instability of the subject during video recording, which superimposes a certain level of inaccuracy and noise onto the acquired signal as shown in Fig.9 (left).

Preprints (www.preprints.org) | NOT PEER-REVIEWED | Posted: 17 August 2018 doi:10.20944/preprints201808.0295.v1

Peer-reviewed version available at Methods Protoc. 2018, 1, 39; doi:10.3390/mps1040039



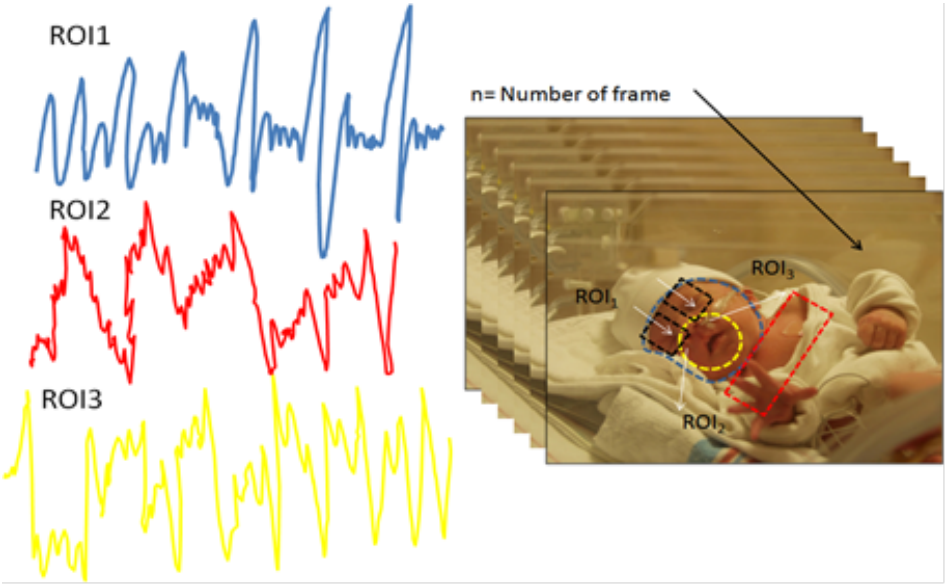


**Figure 10.** (Left) Extracted gradient movement from defined ROIs based on color intensity variation in successive video frames. (Right) Video frame series of the neonate inside the incubator with three defined ROI profiles over forehead, nose, and shoulder.

### *2.6. Monitoring Behavior and Emotion of Neonates*

Technologies that can monitor movements and other physiomarkers are promising tools for assessing a newborn's emotional status. They can record the responses of newborn to pleasant or stressful stimuli, approximate pain scores, and observe any abnormal movements [34,70]. The only technique presently used to assess neonatal behavior and emotional response is electroencephalography (EEG), which is a broad and general method for detecting and classifying these complex patterns. Alternatively, a group of light-emitting diodes can be attached to the upper and lower limbs of preterm infants and recorded continuously by a remote workstation to assess skeletal-based behavioral patterns as we can noticed in table.2 were many of the detection rate for such related behavioral pattern associated with somatic involvement of the preterm infants. Therefore, developing a new method for quantifying these reactions and responses could be quite advantageous in the assessment of infants for experiencing a variety of emotions including pain.

**Table 2.** tabulation of the behavioral index used in the classification of neonate's movement using IR-kinect detector.

| Behavior index | Detection head% | Detection upper extem.% | Detection lower extem.% |
|---|---|---|---|
| BH1 | 78 | 90 | 91 |
| BH2 | 62 | 92 | 73 |
| BH3 | 79 | 96 | 95 |
| BH4 | 71 | 86 | 93 |
| BH5 | 86 | 93 | 82 |

One of the proposed solutions for such a monitoring strategy is to use a visible camera to detect the pattern of local and global body movements. This monitoring strategy can be achieved by incorporating these detected movements into virtual mechanical-linkage models of the neonate. Converting the linkage models into meaningful biomechanical data can be a very useful method for assessing neonatal behavior and developing clinical applications. Fig.11 illustrates how a Microsoft Kinect® [71] device can be connected to the infant warmer to monitor and analyze the infant's movements.

Preprints (www.preprints.org) | NOT PEER-REVIEWED | Posted: 17 August 2018 doi:10.20944/preprints201808.0295.v1

Peer-reviewed version available at Methods Protoc. 2018, 1, 39; doi:10.3390/mps1040039



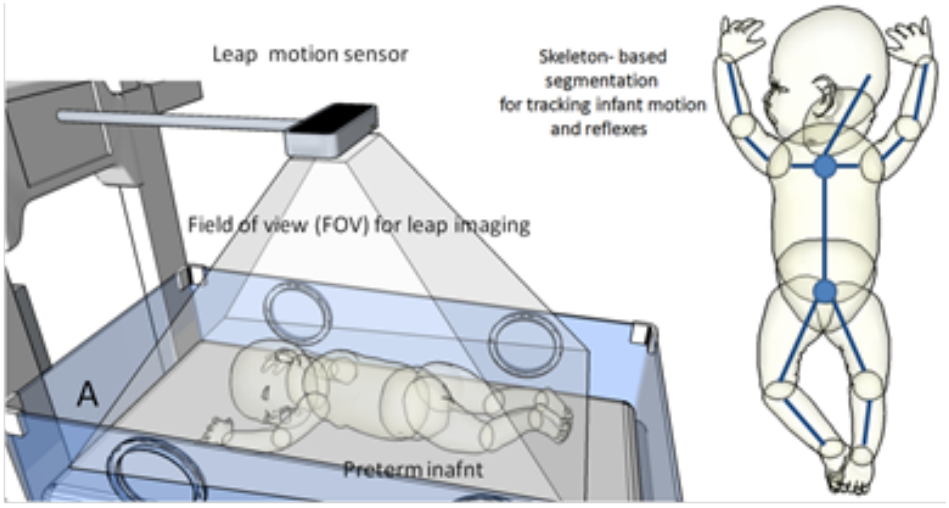


**Figure 12.** Experimental setup of a LeapMotion[ő] unit to monitor body movements of the neonate.

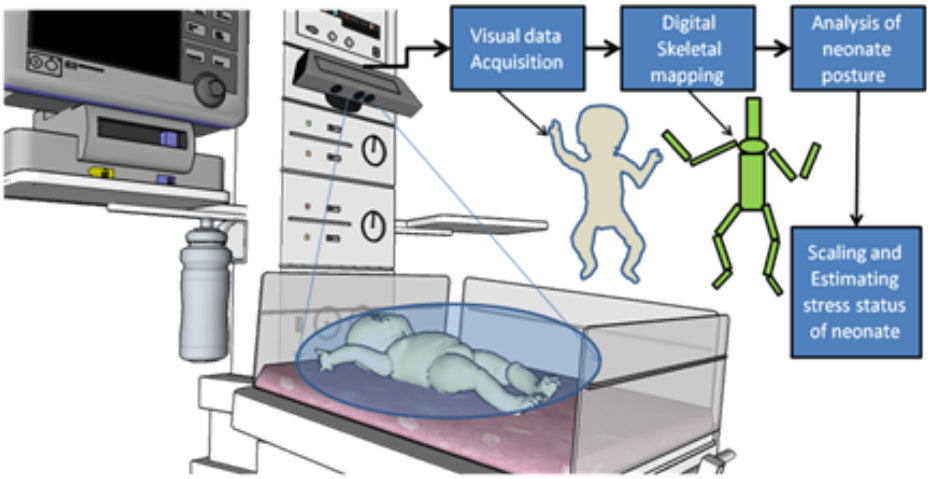


**Figure 11.** Microsoft Kinect experimental setup for mapping a neonate under intensive care, and estimation of behavioral patterns of the global and local body movements.

Another modality that can be used to track the neonate's movements is leap motion for virtual reality (VR) (Fig.12). Because the neonate can be as small as a human hand, leap motion can be a very powerful tool for detecting and tracking motion in newborn babies.

### *2.7. Computer generated graphics (CGI) in contactless neonatal imaging*

As development of digital technology has accelerated, so too has the number of applications for computer graphics and computer-generated imagery (CGI). This boom has served to boost the potential application of these technologies in different fields, and the medical field is no exception. There has been great attention paid to these tools in the medical field, and they have become widely used in medical imaging (CT and MR imaging), medical educational simulators, and biomechanical analyses of human body.
This technology could be very useful for neonatal contactless imaging. Specifically, a high-speed camera could be used to image markers that are attached to the neonate's body. These markers can then be segmented and processed in a separate batches of image processing to identify several lo-cal/global regional movements—which will correspond to specific respiratory and pulmonary functions that the technology is intended to identify.

**Table 3.** Physiological parameters that can be inferring from CGI neonatal imaging methods.

| Parameter | Dynamic range | Error percentage % |
|---|---|---|
| Respiration rate (RR) | 10-14 | 0.5-1.4 |
| Heart rate (HR) | 40-85 | 0.2-1 |
| End tidal volume (ETV) | 20-50 mmHg | 3-5 |
| Lung compliance (LC) | 70-90 ml/cm $H_2O$ | 3-6.2 |

Fig. 13 illustrates the basic configuration of such CGI-generated images by using inductive stretched respiratory belt which can be utilized to generate an image revealed the physiological activities associated with the change of spatial coordinate of these strips.

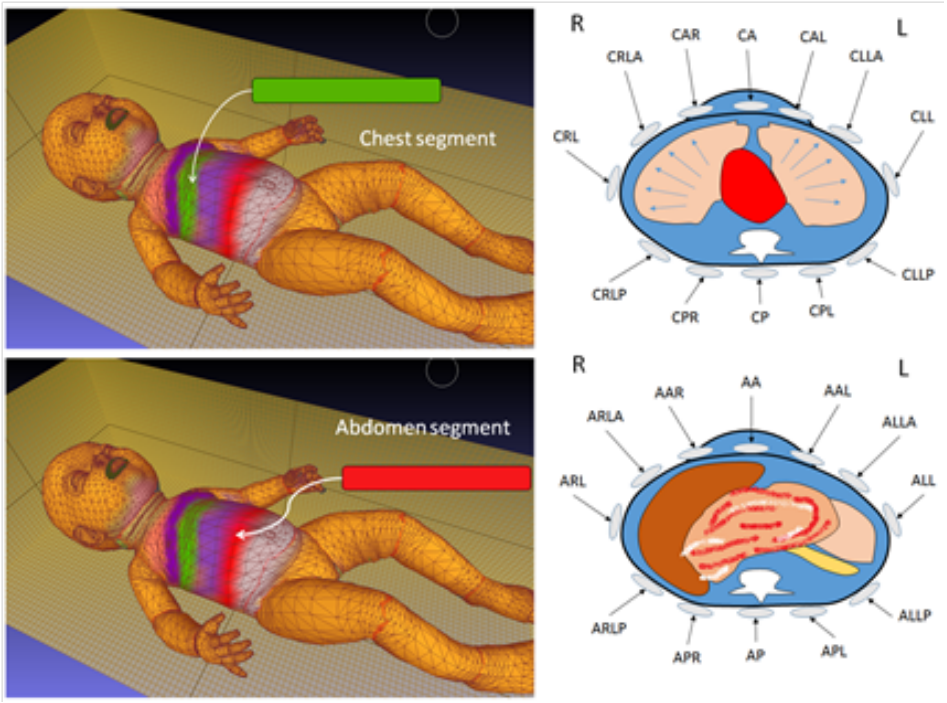


**Figure 13.** Experimental setup for computer-generated imaging (CGI) used in the detection and identification of respiratory and pulmonary functions by using a clinical inductive belt positioned at two levels (upper and lower) to generate several color-coded regions via CGI-vertex meshing colorization to indicate displacement and mechanical distortion due to several physiological- and pathological-related events.

### *2.8. Embedding Contactless Imaging inside an Incubator*

An example of incubator that incorporates various contactless imaging modalities into its hard-ware can be seen in Fig.14. However, this incubator of the future faces one limitation: the level of specific absorption rate (SAR) for all these technologies in the same measurement space that may interfere with each other. This limitation may curtail the extent to which these imaging and diagnostic modules can be used with very small and fragile patients like newborn infants.

Preprints (www.preprints.org) | NOT PEER-REVIEWED | Posted: 17 August 2018 doi:10.20944/preprints201808.0295.v1

Peer-reviewed version available at Methods Protoc. 2018, 1, 39; doi:10.3390/mps1040039



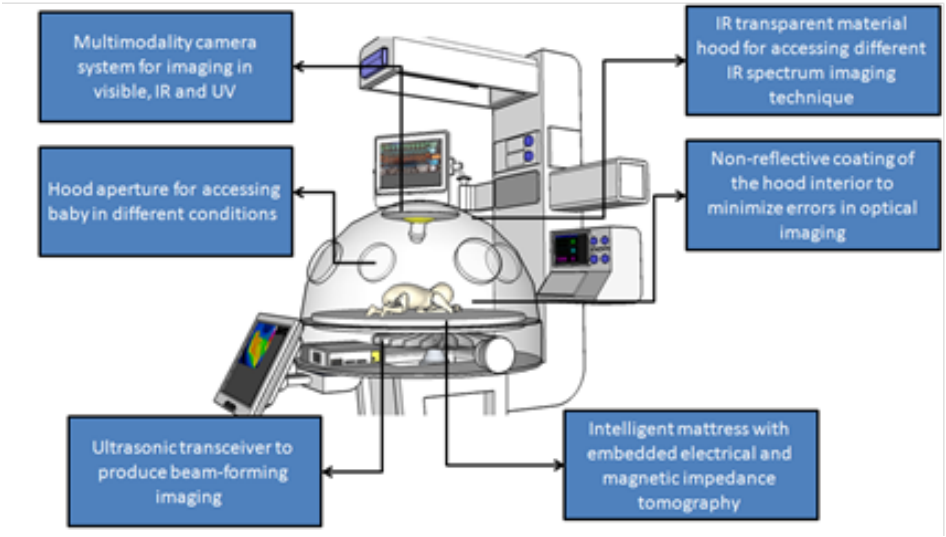


**Figure 14.** A schematic of a neonatal incubator with multiple different embedded contactless imaging modalities for the early detection of various pathologies and neonatal diseases.

### *2.9. Infrared Thermal Tomography Imaging*

This is a modified approach to the conventional thermal imaging, it is proposed to fully accounts for diffusion phenomena in a tomographic imaging proposition. Here, instead of the large area source used in conventional thermal imaging applications, a raster scanned point source is employed in order to provide the well-defined source-receiver positions required for tomographic imaging. An algorithm for the forward propagation problem, based on the Pennes' bioheat transfer (PBHT) method in combination with Galerkin finite element method (FEM), these two mathematical models with the corresponding weak formulation for the thermal diffusion is considered. A thermal diffusion modified version of the algebraic reconstruction technique (ART) is used for tomography approach.

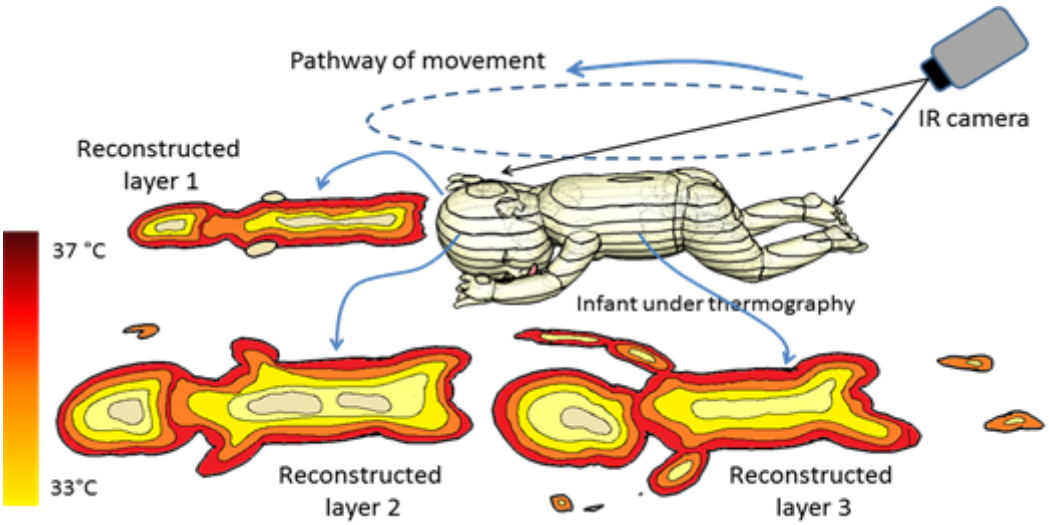


**Figure 15.** Imaging reconstruction of thermal tomography for neonate by using DYTTI method, this gives the physician a clear representation of temperature picture of neonate's body

A Dynamic thermal tomographic imaging (DYTTI) method can be implemented and tested in the basis on inverse mathematical problem such as tomo- or topographic reconstruction method. As of DYTTI

is based on acquisition of the object under test from different angle with time constant less than the 3 second, in order to catch the real-time surface temperature changes throughout the acquisition phase. Thus, providing multi-planar information about 75% of the infant's body and therefore by using inverse thermal reconstruction, we can estimate the obscuring temperature profile of his/her body. Thermal tomography application in neonatology, will gives more quantitative thermal modeling through multiple point temperature registration. This dynamic imaging method will open a door for more complicated clinical monitoring paradigm during neonates care (jaundice, hypothermia, sepsis, meningitis and other infectious diseases). Additionally, estimation of the internal profile temperature will gives the physician a new promising tool for early warning system of any complicated pathologies and disorders.

## 3. Discussion and Conclusions

Contactless neonatal imaging can assert itself as a useful medical tool in the near future if the associated technological and clinical challenges can be addressed. Indeed, contactless imaging is not far from becoming a standard practice in NICUs. The parameters acquired from optical, NIR, SWIR, MWIR and LWIR, and other modalities will be invaluable if they are interpreted in a manner that facilitates more effective clinical decision making in the NICU. Combining two imaging approaches (for example, one passive, like LWIR, and one active, like SWIR) can cover a wider range of physiomarkers and physiofeatures in clinical diagnostics and telehealth systems. Moreover, other computer imaging techniques can be used in conjunction with these contactless technologies. As computer imaging advances alongside contactless imaging, the coordinated use of these technologies (e.g. CGI, motion capturing, 3D augmented reality, etc.) can be helped to produce better contactless imaging and diagnosis of newborn infants and accelerate the future integration of these technologies in the upcoming NICU medical revolution. **Author Contributions:** For research articles with several authors, a short paragraph specifying their individual contributions must be provided. The following statements should be used "Conceptualization, A.A. and Y.E.; wrote the whole paper including Methodology, Software, Validation, Y.E., and A.A.; Formal Analysis, M.N.; Investigation, Y.E.; Resources, M.S.; Data Curation, A.A.; Writing—Original Draft Preparation, G.S.; Writing—Review & Editing, S.S.; Visualization, M.S.; Supervision, M.N.; Project Administration, M.N.; Funding Acquisition, Y.E."

**Funding:** This research received no external funding.

**Conflicts of Interest:** The authors declare no conflict of interest.

1. Clark, R.P. Human Skin Temperature and Its Relevance in Physiology and Clinical Assessment. *Recent Advances in Medical Thermology* **1984**. doi:10.1007/978-1-4684-7697-2_2.
2. Vollmer, M.; Möllmann, K.P. Infrared Thermal Imaging, 2017. doi:10.1002/9783527693306.
3. Bhatia, R.; Schmölzer, G.M.; Davis, P.G.; Tingay, D.G. Electrical impedance tomography can rapidly detect small pneumothoraces in surfactant-depleted piglets. *Intensive Care Medicine* **2012**, *38*, 308. doi:10.1007/s00134-011-2421-z.
4. Burg, P.; Miedema, M.; Jongh, F.; Kaam, A. Correlation between lung volume changes measured by electrical impedance tomography and respiratory inductance plethysmography in high-frequency ventilated preterm infants. *Tijdschrift voor Kindergeneeskunde* **2013**, *81*, 30. doi:10.1007/s12456-013-0030-1.
5. Bayford, R. Basic Electrical Impedance Tomography. *Bioimpedance in Biomedical Applications and Research* **2018**. doi:10.1007/978-3-319-74388-2_3.
6. Luppa, P.B.; Vashist, S.K.; Luong, J.H.T. Non-invasive analysis. *Point-of-Care Testing* **2018**. doi:10.1007/978-3-662-54497-6_11.
7. Ruminski, J.; Kwasniewska, A. Evaluation of Respiration Rate Using Thermal Imaging in Mobile Conditions. In *Application of Infrared to Biomedical Sciences*; Springer, 2017. doi:10.1007/978-981-10-3147-2_18.
8. Abbas, A.K.; Heimann, K.; Jergus, K.; Orlikowsky, T.; Leonhardt, S. Neonatal non-contact respiratory monitoring based on real-time infrared thermography. *BioMedical Engineering OnLine* **2011**, *10*, 1. doi:10.1186/1475-925X-10-93.
9. Arridge, S.R. Optical tomography in medical imaging. *Inverse problems* **1999**, *15*, R41.
10. Goswami, D.K.; Vener, D.F. Pediatric Cardiovascular Monitoring. *Congenital Heart Disease in Pediatric and Adult Patients* **2017**. doi:10.1007/978-3-319-44691-2_7.

11. Abbas, A.K.; Heiman, K.; Jergus, K.; Orlikowsky, T.; Leonhardt, S. *Neonatal Infrared Thermography Monitoring (Book chapter) in Neonatal Monitoring Technologies: Design for Integrated Solutions: Design for Integrated Solutions*, 1 ed.; Number 1 in Premier reference source, Medical Information Science Reference, 2012.
12. Holst, G.C. *Common sense approach to thermal imaging*; SPIE: Bellingham, 2000. Literaturangaben.
13. Pascoe, D.D. Potential Errors in Mean Skin Temperature Calculation Due to Thermistor Placement as Determined by Infrared Thermography. *Agache's Measuring the Skin* **2017**. doi:10.1007/978-3-319-32383-1_75.
14. Caniou, J. Infrared detection. *Passive Infrared Detection* **1999**. doi:10.1007/978-1-4757-6140-5_1.
15. Abbas, A.K.; Heimann, K.; Blazek, V.; Orlikowsky, T.; Leonhardt, S. Neonatal infrared thermography imaging: Analysis of heat flux during different clinical scenarios **2012**. *55*, 538–548. doi:10.1016/j.infrared.2012.07.001.
16. Amri, A.; Wilkinson, A.J.; Pulko, S.H. Potentialities of Dynamic Breast Thermography. In *Application of Infrared to Biomedical Sciences*; Springer, 2017. doi:10.1007/978-981-10-3147-2_7.
17. Bührer, C.; Zimmermann, A. Management of very preterm newborn infants (VLBW, ELBW). doi:10.1017/cbo9781139010467.043.
18. Gade, R.; Moeslund, T.B. Constrained multi-target tracking for team sports activities. *IPSJ Transactions on Computer Vision and Applications* **2018**, *10*, 1. doi:10.1186/s41074-017-0038-z.
19. Diakides, N.; Bronzino, J. Medical Infrared Imaging, 2007. doi:10.1201/9781420008340.
20. Abbas, A.K. *Infrared thermography imaging for contactless neonatal monitoring and care*; Number 24 in Aachener Beiträge zur Medizintechnik, Shaker: Aachen, 2015.
21. Amri, A.; Wilkinson, A.J.; Pulko, S.H. Potentialities of Dynamic Breast Thermography. In *Application of Infrared to Biomedical Sciences*; Springer, 2017. doi:10.1007/978-981-10-3147-2_7.
22. Martini, S.; Corvaglia, L. Splanchnic NIRS monitoring in neonatal care: rationale, current applications and future perspectives. *Journal of Perinatology* **2018**, *38*, 431. doi:10.1038/s41372-018-0075-1.
23. Abbas, A.K.; Leonhardt, S. Intelligent neonatal monitoring based on a virtual thermal sensor. *BMC Medical Imaging* **2014**, *14*, 1. doi:10.1186/1471-2342-14-9.
24. Knobel, R.B.; Guenther, B.D.; Rice, H.E. Thermoregulation and thermography in neonatal physiology and disease. *Biological research for nursing* **2011**, *13*, 274–282.
25. Saxena, A.K.; Willital, G.H. Infrared thermography: Experience from a decade of pediatric imaging. *European Journal of Pediatrics* **2008**, *167*, 757–764. doi:10.1007/s00431-007-0583-z.
26. Nikolai Blanik, Abbas K. Abbas, B.V.V.B.S.L. Hybrid optical imaging technology for long-term remote monitoring of skin perfusion and temperature behavior. *Journal of Biomedical Optics* **2014**, *19*, 19 – 19 – 11. doi:10.1117/1.JBO.19.1.016012.
27. Andropoulos, D.B.; Stayer, S.A.; McKenzie, E.; Fraser, C.D. Novel cerebral physiologic monitoring to guide low-flow cerebral perfusion during neonatal aortic arch reconstruction. *The Journal of Thoracic and Cardiovascular Surgery* **2003**, *125*, 491 – 499. doi:https://doi.org/10.1067/mtc.2003.159.
28. Arridge, S.R.; Hebden, J.C. Optical imaging in medicine: II. Modelling and reconstruction. *Physics in Medicine & Biology* **1997**, *42*, 841.
29. Langston, T. Reflectance-based skin detection in the short wave infrared band and its application to video. *Journal of Applied Remote Sensing* **2016**, *10*, 10 – 10 – 25. doi:10.1117/1.JRS.10.046026.
30. Donges, A.; Noll, R. Detection of Electromagnetic Radiation. In *Laser Measurement Technology*; Springer, 2015. doi:10.1007/978-3-662-43634-9_5.
31. Alpar, O.; Krejcar, O. Detection of Irregular Thermoregulation in Hand Thermography by Fuzzy C-Means. *Bioinformatics and Biomedical Engineering* **2018**. doi:10.1007/978-3-319-78759-6_24.
32. Gade, R.; Moeslund, T.B. Thermal cameras and applications: a survey. *Machine Vision and Applications* **2014**, *25*, 245. doi:10.1007/s00138-013-0570-5.
33. Nakamura, H. Development of noninvasive measurement of peripheral circulation and its medical application. *Environmental Health and Preventive Medicine* **1997**, *2*, 1. doi:10.1007/BF02931222.
34. Gunnar, M.R.; Porter, F.L.; Wolf, C.M.; Rigatuso, J.; Larson, M.C. Neonatal Stress Reactivity: Predictions to Later Emotional Temperament. *Child Development*, *66*, 1–13, [https://onlinelibrary.wiley.com/doi/pdf/10.1111/j.1467-8624.1995.tb00851.x]. doi:10.1111/j.1467-8624.1995.tb00851.x.
35. VandenBerg, K.A. Individualized developmental care for high risk newborns in the NICU: A practice guideline. *Early Human Development* **2007**, *83*, 433 – 442. doi:https://doi.org/10.1016/j.earlhumdev.2007.03.008.
36. Keiser, G. Light-Tissue Interactions. In *Biophotonics*; Springer, 2016. doi:10.1007/978-981-10-0945-7_6.

37. Nishimura, E.M.; Rapoport, E.D.; Wubbels, P.M.; Downs, T.H.; Downs, J. Hunter, I. Functional Near-Infrared Sensing (fNIR) and Environmental Control Applications. In *Brain-Computer Interfaces*; Springer, 2010. doi:10.1007/978-1-84996-272-8_8.
38. Beyerer, J.; Puente León, F.; Frese, C. Radiometry. In *Machine Vision*; Springer, 2016. doi:10.1007/978-3-662-47794-6_4.
39. Figueiredo, J.L.; Siegel, C.; Nahrendorf, M.; Weissleder, R. Intraoperative Near-Infrared Fluorescent Cholangiography (NIRFC) in Mouse Models of Bile Duct Injury. *World Journal of Surgery* **2010**, *34*, 336. doi:10.1007/s00268-009-0332-8.
40. Benaron, D.A.; Stevenson, D.K. Resolution of Near Infrared Time-of-Flight Brain Oxygenation Imaging. In *Oxygen Transport to Tissue XV*; Springer, 1994. doi:10.1007/978-1-4615-2468-7_81.
41. Hebden, J.C.; Austin, T. Optical tomography of the neonatal brain. *European Radiology* **2007**, *17*, 2926. doi:10.1007/s00330-007-0659-1.
42. Tibby, S.M. Hemodynamic Monitoring. In *Cardiovascular Pediatric Critical Illness and Injury*; Springer, 2009. doi:10.1007/978-1-84800-923-3_2.
43. HEAT TRANSFER IN AGITATED VESSELS. doi:10.1615/atoz.h.heat_transfer_in_agitated_vessels.
44. Keiser, G. Overview of Biophotonics. In *Biophotonics*; Springer, 2016. doi:10.1007/978-981-10-0945-7_1.
45. Hespos, S.J.; Ferry, A.L.; Cannistraci, C.J.; Gore, J.; Park, S. Using Optical Imaging to Investigate Functional Cortical Activity in Human Infants. In *Imaging the Brain with Optical Methods*; Springer, 2010. doi:10.1007/978-1-4419-0452-2_8.
46. Takeuchi, M.; Hori, E.; Takamoto, K.; Tran, A.H.; Satoru, K.; Ishikawa, A.; Ono, T.; Endo, S.; Nishijo, H. Brain Cortical Mapping by Simultaneous Recording of Functional Near Infrared Spectroscopy and Electroencephalograms from the Whole Brain During Right Median Nerve Stimulation. *Brain Topography* **2009**, *22*, 197. doi:10.1007/s10548-009-0109-2.
47. Cholewka, A.; Kajewska, J.; Marek, K.; Sieroń-Stołtny, K.; Stanek, A. How to use thermal imaging in venous insufficiency? *Journal of Thermal Analysis and Calorimetry* **2017**, *130*, 1317. doi:10.1007/s10973-017-6141-7.
48. Lytvynchuk, L.; Glittenberg, C.; Binder, S. Intraoperative Spectral Domain Optical Coherence Tomography: Technology, Applications, and Future Perspectives. *Spectral Domain Optical Coherence Tomography in Macular Diseases* **2017**. doi:10.1007/978-81-322-3610-8_29.
49. Visscher, M.O.; Adams, D.M.; Burkes, S.A. Dynamic Infrared Thermography of Infantile Hemangiomas. In *Agache's Measuring the Skin*; Springer, 2017. doi:10.1007/978-3-319-32383-1_150.
50. Herrin, J.T. Management of Fluid and Electrolyte Abnormalities in Children. *Core Concepts in the Disorders of Fluid, Electrolytes and Acid-Base Balance* **2013**. doi:10.1007/978-1-4614-3770-3_5.
51. Naga, O. Fetus and Newborn Infants (Neonatology). *Pediatric Board Study Guide* **2015**. doi:10.1007/978-3-319-10115-6_8.
52. Antonutto, G.; Girardis, M.; Tuniz, D.; Prampero, P.E. Noninvasive assessment of cardiac output from arterial pressure profiles during exercise. *European Journal of Applied Physiology and Occupational Physiology* **1995**, *72*, 18. doi:10.1007/BF00964109.
53. Tamura, T.; Maeda, Y. Photoplethysmogram. In *Seamless Healthcare Monitoring*; Springer, 2018. doi:10.1007/978-3-319-69362-0_6.
54. Böhringer, H.J.; Lankenau, E.; Stellmacher, F.; Reusche, E.; Hüttmann, G.; Giese, A. Imaging of human brain tumor tissue by near-infrared laser coherence tomography. *Acta Neurochirurgica* **2009**, *151*, 507. doi:10.1007/s00701-009-0248-y.
55. Benaron, D.A.; Hintz, S.R.; Villringer, A.; Boas, D.; Kleinschmidt, A.; Frahm, J.; Hirth, C.; Obrig, H.; van Houten, J.C.; Kermit, E.L.; others. Noninvasive functional imaging of human brain using light. *Journal of Cerebral Blood Flow & Metabolism* **2000**, *20*, 469–477.
56. Lal, R.; Nicoud, F.; Bars, E.L.; Deverdun, J.; Molino, F.; Costalat, V.; Mohammadi, B. Non Invasive Blood Flow Features Estimation in Cerebral Arteries from Uncertain Medical Data. *Annals of Biomedical Engineering* **2017**, *45*, 2574. doi:10.1007/s10439-017-1904-7.
57. Mariotti, A.; Grossi, G.; Amerio, P.; Orlando, G.; Mattei, P.A.; Tulli, A.; Romani, G.L.; Merla, A. Finger Thermoregulatory Model Assessing Functional Impairment in Raynaud's Phenomenon. *Annals of Biomedical Engineering* **2009**, *37*, 2631. doi:10.1007/s10439-009-9788-9.
58. Arzani, A.; Dyverfeldt, P.; Ebbers, T.; Shadden, S.C. In Vivo Validation of Numerical Prediction for Turbulence Intensity in an Aortic Coarctation. *Annals of Biomedical Engineering* **2012**, *40*, 860. doi:10.1007/s10439-011-0447-6.

59. Gao, L.; ElwellElwell, C.E.; Kohl-Bareis, M.; Gramer, M.; Cooper, C.E.; Leung, T.S.; Tachtsidis, I. Effects of Assuming Constant Optical Scattering on Haemoglobin Concentration Measurements Using NIRS during a Valsalva Manoeuvre. *Oxygen Transport to Tissue XXXII* **2011**. doi:10.1007/978-1-4419-7756-4_3.
60. McGah, P.M.; Levitt, M.R.; Barbour, M.C.; Morton, R.P.; Nerva, J.D.; Mourad, P.D.; Ghodke, B.V.; Hallam, D.K.; Sekhar, L.N.; Kim, L.J.; Aliseda, A. Accuracy of Computational Cerebral Aneurysm Hemodynamics Using Patient-Specific Endovascular Measurements. *Annals of Biomedical Engineering* **2014**, *42*, 503. doi:10.1007/s10439-013-0930-3.
61. Paul, M.; Venema, B.; Blazek, V.; Mühlsteff, J.; Leonhardt, S. A camera-based multispectral setup for remote vital signs assessment. *EMBEC & NBC 2017* **2018**. doi:10.1007/978-981-10-5122-7_242.
62. Ospina-Restrepo, L.C.; Herrera-Velasquez, L.M.; Barrera-Causil, C.J.; Fandiño-Toro, H.A.; Ramirez-Arbelaez, L.M. Thermoregulation of the hand: assessment with infrared thermography. In *VII Latin American Congress on Biomedical Engineering CLAIB 2016, Bucaramanga, Santander, Colombia, October 26th -28th, 2016*; Springer, 2017. doi:10.1007/978-981-10-4086-3_182.
63. Ring, F.J. Skin Thermal Imaging. In *Agache's Measuring the Skin*; Springer, 2017. doi:10.1007/978-3-319-32383-1_73.
64. Benni, P.B.; MacLeod, D.; Ikeda, K.; Lin, H.M. A validation method for near-infrared spectroscopy based tissue oximeters for cerebral and somatic tissue oxygen saturation measurements. *Journal of Clinical Monitoring and Computing* **2018**, *32*, 269. doi:10.1007/s10877-017-0015-1.
65. Huppert, T.J. History of Diffuse Optical Spectroscopy of Human Tissue. *Optical Methods and Instrumentation in Brain Imaging and Therapy* **2013**. doi:10.1007/978-1-4614-4978-2_2.
66. Alpar, O.; Krejcar, O. Quantization and Equalization of Pseudocolor Images in Hand Thermography. *Bioinformatics and Biomedical Engineering* **2017**. doi:10.1007/978-3-319-56148-6_35.
67. Li, D.; Chen, B.; Wu, W.; Ying, Z. Experimental investigation on the vascular thermal response to near-infrared laser pulses. *Lasers in Medical Science* **2017**, *32*, 2023. doi:10.1007/s10103-017-2311-x.
68. Soerensen, D.D.; Pedersen, L.J. Infrared skin temperature measurements for monitoring health in pigs: a review. *Acta Veterinaria Scandinavica* **2015**, *57*, 1. doi:10.1186/s13028-015-0094-2.
69. St. Lawrence, K.; Verdecchia, K.; Elliott, J.; Diop, M. Measuring Cerebral Hemodynamics and Energy Metabolism by Near-Infrared Spectroscopy. *Brain Energy Metabolism* **2014**. doi:10.1007/978-1-4939-1059-5_12.
70. Wang, J.; Lu, G.; Jing, X.; Zhang, Y.; Lv, H. Study of the Ballistocardiogram signal in non-contact life detection system based on radar. In *7th Asian-Pacific Conference on Medical and Biological Engineering*; Springer, 2008. doi:10.1007/978-3-540-79039-6_149.
71. Abbas, A.K.; Leonhardt, S. Intelligent neonatal monitoring based on a virtual thermal sensor. *BMC Medical Imaging* **2014**, *14*, 1. doi:10.1186/1471-2342-14-9.